New Phytologist

Research

# A transcriptional repressor HVA regulates vascular bundle formation through auxin transport in *Arabidopsis* stem

**Qian Du[1]*, Bingjian Yuan[1]*, Gaurav Thapa Chhetri[1]*, Tong Wang[1], Liying Qi[1] and Huanzhong Wang[1,2]**

[1]Department of Plant Science and Landscape Architecture, University of Connecticut, 1376 Storrs Rd, Storrs, CT 06269, USA; [2]Institute for System Genomics, University of Connecticut, Storrs, CT 06269, USA

Author for correspondence:
*Huanzhong Wang*
*Email:* huanzhong.wang@uconn.edu

Received: *29 April 2024*
Accepted: *2 July 2024*

*New Phytologist* (2024)
**doi**: 10.1111/nph.19970

**Key words:** *Arabidopsis*, cambium activity, regulation, transcription factor, vascular development.

## Summary

- Vascular bundles transport water and photosynthate to all organs, and increased bundle number contributes to crop lodging resistance. However, the regulation of vascular bundle formation is poorly understood in the Arabidopsis stem.
- We report a novel semi-dominant mutant with high vascular activity, *hva-d*, showing increased vascular bundle number and enhanced cambium proliferation in the stem. The activation of a C2H2 zinc finger transcription factor, *AT5G27880/HVA*, is responsible for the *hva-d* phenotype. Genetic, biochemical, and fluorescent microscopic analyses were used to dissect the functions of HVA.
- HVA functions as a repressor and interacts with TOPLESS via the conserved Ethylene-responsive element binding factor-associated Amphiphilic Repression motif. In contrast to the HVA activation line, knockout of *HVA* function with a CRISPR-Cas9 approach or expression of HVA fused with an activation domain VP16 (*HVA-VP16*) resulted in fewer vascular bundles. Further, HVA directly regulates the expression of the auxin transport efflux facilitator *PIN1*, as a result affecting auxin accumulation. Genetics analysis demonstrated that PIN1 is epistatic to HVA in controlling bundle number.
- This research identifies HVA as a positive regulator of vascular initiation through negatively modulating auxin transport and sheds new light on the mechanism of bundle formation in the stem.

## Introduction

Vascular tissues are organized as bundles in stems of both monocotyledonous and dicotyledonous plants. Lodging resistance and crop production are positively related to increased vascular bundles in cereal crops (Fujita *et al.*, 2013; Wang & Wang, 2020). The *Arabidopsis* stem shows a developmental gradient from top to bottom. Discrete vascular bundles can be observed at the stem periphery a few centimeters below the shoot apical meristem (SAM). Each vascular bundle is composed of protoxylem cells, protophloem, and intervening procambial cells. In the middle part of the stem, meristematic cells from vascular bundles (fascicular) and interfascicular regions connect and form a ring-shaped cambium. At the bottom of the stem, cambial cells proliferate and then differentiate into secondary xylem and secondary phloem, forming a stem structure similar to tree species. The Arabidopsis stem develops five to eight vascular bundles under long-day conditions. However, the mechanisms for regulating vascular bundle formation and cambium activity are not well-understood (Miyashima *et al.*, 2013; Tonn & Greb, 2017; Wang & Wang, 2020; Hunziker & Greb, 2024; Wang, 2024).

Our understanding of vascular formation in plant postembryonic tissues is mainly derived from studies of roots and leaves. In primary roots, xylem and pluripotent procambial cells are produced directly from vascular initials touching the quiescent center (Mahonen *et al.*, 2000; Ohashi-Ito *et al.*, 2014). In developing leaves, new veins develop from vascular preprocambium cells, which are iteratively recruited from parenchyma cells (Miyashima *et al.*, 2013). An auxin-canalization hypothesis has been proposed to explain the formation of the vascular system in leaves (Sachs, 1981; Rolland-Lagan & Prusinkiewicz, 2005). According to this theory, auxin flow is directed by the polar localization of auxin efflux carrier PINFORMED1 (PIN1) (Scarpella *et al.*, 2006), which in turn defines the position of procambium precursor strands in a self-reinforcing fashion (Sachs, 2000). The expression of *PIN1* (Wenzel *et al.*, 2007) and auxin synthesis genes (Cheng *et al.*, 2006) are essential to this process. Overexpression of *KANADI* (*KAN*) genes reduces *PIN1* expression and auxin level, therefore suppressing procambial cell formation (Ilegems *et al.*, 2010). KAN interplays with class III HD-ZIP transcription factors (TFs) in vascular development. *ATHB8* is one of the five HD-ZIP III genes specifically expressed in procambium precursor and procambial cells (Baima *et al.*, 1995; Donner *et al.*, 2009). ATHB8 confines procambium precursor cells to continuous and narrow regions by reducing the

*These authors contributed equally to this work.

sensitivity to auxin in terms of *PIN1* expression (Donner *et al.*, 2009). Other plant hormones, such as cytokinin and brassinosteroid, also play critical roles in vascular development in roots and leaves (Cano-Delgado *et al.*, 2010).

Auxin plays critical roles in vascular initiation and development in the stem. Previous studies revealed that auxin distribution peaked in developing cambium in woody plants (Tuominen *et al.*, 1997). In the Arabidopsis stem, the active auxin form indole-3-acetic acid (IAA) is sufficient to promote procambial cells proliferation and xylem differentiation (Agusti *et al.*, 2011; Suer *et al.*, 2011; Fàbregas *et al.*, 2015). A mathematical model predicted that auxin maxima controlled by polar transportation determine vascular bundle position and spacing in the stem (Ibañes *et al.*, 2009). An auxin-response reporter, *DR5::GUS*, was specifically expressed in the position of vascular bundles (Fàbregas *et al.*, 2010). Furthermore, mutants of auxin efflux carrier *PIN1* showed an increased number of vascular bundles in the stem (Turner & Sieburth, 2003). Therefore, auxin transport controls auxin distribution and vascular bundle patterning in stems.

Proteins with an Ethylene-responsive element binding factor-associated Amphiphilic Repression (EAR) motif often function as transcription repressors (Ohta *et al.*, 2001). The EAR motif was initially identified in members of the Arabidopsis ethylene response factor (ERF) and later found in transcription factors participating in other crucial developmental pathways, such as IAA proteins in auxin signaling (Tiwari *et al.*, 2004), BES1 and BZR1 in brassinosteroid (BR) signaling (Yin *et al.*, 2002; He *et al.*, 2005), and SUPERMAN (SUP) in flower development (Hiratsu *et al.*, 2002). The consensus sequences for the EAR motif are predominantly either LxLxL or DLNxxP (Kagale & Rozwadowski, 2011). Transcription repressors with EAR motif interact with corepressors, such as TOPLESS (TPL) (Wang *et al.*, 2013; Ke *et al.*, 2015) and AtSAP18 (Song & Galbraith, 2006), therefore affecting histone modifications and repressing gene transcription. In Arabidopsis, the *topless-1* (*tpl-1*) mutation transforms the shoot pole into a second root pole (Long *et al.*, 2006). The asparagine to histidine mutation at position 176 results in a dominant-negative effect (Osmont & Hardtke, 2008).

In this paper, we report the identification of a unique semi-dominant mutant *hva-d*, showing High Vascular meristem Activity (HVA) in both primary and secondary stems. The *HVA* gene encodes a novel zinc finger transcription factor with a C-terminal EAR motif. HVA is localized in the nucleus and functions as a transcriptional repressor through interaction with a corepressor TPL. Further, HVA directly regulates the expression of *PIN1*, resulting in altered auxin distribution in the stem. This research identifies a regulator of vascular bundle formation and sheds light on the regulation of vascular formation and patterning in *Arabidopsis* stem.

## Materials and Methods

### Plant materials and growth conditions

*Arabidopsis thaliana* L. ecotype Col–0 and *Landsberg erecta* (*Ler*) were used in this study as wild-type (WT) controls and as the genetic backgrounds. *Nicotiana benthamiana* L. was used in this study for bimolecular fluorescence complementation (BiFC) assay. Mutant lines *pin1*, *PIN1::PIN1-GFP* were obtained from *Arabidopsis* Biological Resource Center. Reporter lines *ProDR5rev2::GFP* and *ProAtHB8::YFP* were kindly provided by Dr Thomas Greb; *ProAPL::GUS* was received from Dr Yrjo Helariutta; *ProAtHB8::GUS* was received from Dr Li-Jia Qu. The *hva-d* mutant was identified from a large-scale mutant screening using UV microscopy. *Arabidopsis* seeds were sterilized and germinated in media (pH 5.7) containing ½-strength Murashige & Skoog medium (½MS) salts. Plants were grown in growth chambers under the following conditions: 16 h : 8 h, 22°C : 20°C, light : dark.

### Plasmid rescue

The plasmid sequences in pSKI015 flanked by several restriction enzyme sites that can be used for the rescue of T-DNA and adjacent plant sequences from transformed plants as described (Weigel *et al.*, 2000). Three micrograms of genomic DNA, purified with the DNeasy® Plant Mini Kit (Qiagen) and eluted with ddH2O, was digested with KpnI (New England Biolabs, Ipswich, MA, USA) for 3 h. The digested genomic DNA was harvested by phenol–chloroform extraction and was ligated with 1uL of T4 DNA ligase (New England Biolabs) in 10 µl final volume at 16°C overnight. The ligation system was transformed into *E. coli* by a heat shock. Transformed bacteria were plated onto LB agar media supplemented with 100 µg $ml^{-1}$ ampicillin. The purified plasmids were send for sequencing to obtain detailed information about the insertion sites by using the left border primers.

### Constructs and plant transformation

To produce the HVA overexpression construct, we cloned the genomic sequence of *HVA* into the pENTR/D vector and confirmed the accuracy through Sanger sequencing. Primers used for gene cloning and expression analyses can be found in Supporting Information Table S1. The genomic *HVA* was ligated into the XmaI and SacI restriction sites of binary vector pBIG-4 × 35S vector. Plants were transformed by Agrobacterium-mediated transformation. Seeds were selected on plates supplied with 25 µg $l^{-1}$ kanamycin. Resistant plants were transferred to freshly prepared soil. To analyze the subcellular localization of HVA, we inserted the coding sequences of *HVA* gene in-frame with the N-terminal GFP fusion driven by CaMV 35S promoter in the pK7WGF2 vector. The sequence-confirmed constructs were transformed into GV3101 Agrobacterium cells, which were then used to transform WT plants. After antibiotic selection, 5-d-old seedlings were used for observation under a Nikon A1R Spectral Confocal microscope.

### Real-time PCR

Total RNA from the frozen material was extracted using NucleoSpin® RNA extraction kit (Macherey Nagel, Düren, Germany). To eliminate the contamination of genomic DNA, total RNA was treated with DNase for 15 min before elution.

2 μg of total RNA was reverse transcribed using the Maxima Reverse Transcriptase (Thermo Scientific, Waltham, MA, USA) in a 20uL reaction. The cDNA was diluted five times and later used as the template for Quantitative reverse transcription polymerase chain reaction. The cDNA samples were used for quantitative reverse transcription polymerase chain reaction with technical duplicates. The 10 μl reaction included 2 μl of primers (1 μM of each primer), 5 μl of Universal SYBR® Green Supermix (BioRad), 1 μl of diluted cDNA, and 2 μl of water. The PCR program was set according to the manufacturer's instructions (BioRad). Transcript levels were determined by relative quantification using *Arabidopsis UBQ5* gene as a reference.

### Yeast two-hybrid assay

Yeast two-hybrid assays were performed with the GAL4 Two-Hybrid System (Clontech, Mountain View, CA, USA). The entire coding regions of the TPL, HVA, and HVAΔEAR proteins were introduced into the pGADT7 and pGBKT7 vectors (Clontech) by restriction enzyme digestion. Prey (TPL) was expressed as Gal4-DNA-BD fusion proteins in the pGBKT7 plasmid and transformed into YH2Gold yeast strain; preys (HVA and HVAΔEAR) were expressed as Gal4-AD fusion proteins in pGADT7 vector and transformed into the Y187 strain. Bait- and prey-transformed strains were mated, and the resulting diploids were cultured in SD-Leu/−Trp medium. The diploids grew and checked for protein interactions in SD-Leu/−Trp/-His/X-α-gal medium tenfold serial dilutions using distilled water. The interaction between P52 and T proteins was used as a positive control; lam and T protein were employed as negative controls.

### Bimolecular fluorescence complementation assay (BiFC)

For the BiFC constructs, coding sequences of HVA, HVA-ΔEAR, and TPL were amplified by PCR and cloned into the pENTR/D vector. After sequencing confirmation, corresponding genes were subcloned into the destination vector pUBQ-n-YFP and pUBQ-c-YFP through LR reactions using the LR Clonase II (Invitrogen, http://www.invitrogen.com). The destination vector plasmids were then transformed into the *A. tumefaciens* GV3101 strain. To perform the BiFC analysis, cultures of agrobacteria harboring different combinations of HVA and TPL genes were infiltrated into *N. benthamiana* leaves. The p19 protein was used to suppress gene silencing. Leaves were observed under Nikon A1R Spectral Confocal microscope three days after infiltration.

### Histochemical staining

Phloroglucinol-HCl reagent was prepared by mixing 2 volumes of 2% (w/v) phloroglucinol in 95% (v/v) ethanol with 1 volume of concentrated HCl. Cross sections were stained for 1–2 min, washed twice with water, and photographed immediately. The cross-sectional specimens were obtained from Leica VT1000 S Vibrating Blade Microtome (Wetzlar, Germany). The microscope used is Nikon Fluorescence Microscope, and the photographs were captured by Lumenera's INFINITY ANALYZE Software.

### GUS staining

Freshly sectioned stem samples were transferred to staining solution (50 mM NaHPO4 buffer pH 7.2, 2 mM potassium ferricyanide, 2 mM potassium ferrocyanide, and 2 mM X-glucuronide). Samples were placed at 37°C overnight and were incubated 70% ethanol until visualization with a microscope.

### Microarray analysis

A microarray analysis was performed to compare the transcriptomes of the WT and the *hva-dl*/+ heterozygous lines. All plants were grown under long-day conditions for 5 wk. Three biological replicates were used for microarray analysis. Total RNA was isolated using an RNA isolation kit (Qiagen). The Affymetrix Gene Atlas System was used to perform the microarray analysis. The GeneAtlas® WT Expression Kit (Life Technologies Corp., Grand Island, NY, USA) was used for RNA treatment, cDNA synthesis, fragmentation, and labeling. Background correction, quantile normalization, and gene expression analysis were performed using the Transcriptome Analysis Console from Affymetrix. The gene-level differential expression filter was set at Fold Change (linear) and ANOVA *P*-value (condition pair) < 0.05. Selected genes were then validated independently with real-time reverse transcription PCR experiments. The microarray results have been deposited at ArrayExpress with the accession no. EMTAB- 12850.

### Transient repressive expression and dual-luciferase assay

Leaves from healthy *Arabidopsis* plants were cut into 0.5–1-mm strips with razor blades. The leaf strips were put into an enzyme solution containing cellulase and macerozyme, then vacuum-infiltrated for 30 min, followed by digestion for 3 h without shaking in the dark. The protoplasts were filtered with nylon mesh, collected, and transformed by PEG-mediated transfection.

For effector plasmids, the coding sequences of *HVA*, *HVA-ΔEAR*, and *HVAmtEAR* were first cloned into pGBKT7. Then, the coding regions of BD fusion were amplified using specific primers and cloned into p2GW7 using LR Clonase II to yield effector plasmids. Transient expression assays were performed with Arabidopsis protoplasts. Each transformation used 5 μg of reporter plasmid and 4 μg of effector plasmid. For normalization of reporter gene activity, 0.5 μg of plasmid pRLC was used as an internal control. The luciferase activity was detected by Dual-Luciferase® Reporter Assay System (Promega) and analyzed by GloMax® 96 Microplate Luminometer (Promega).

### Chromatin Immunoprecipitation (ChIP) assay

Chromatin Immunoprecipitation (ChIP) experiments were conducted as described previously with minor adjustments (Sun *et al.*, 2024). Stem samples from P*ro35S::GFP-HVA* transgenic plants and the control *Pro35S::YFP* were collected and cut to 0.5-cm segments. The samples were cross-linked with 1% formaldehyde using vacuum infiltration, and then ground to a fine powder with mortar and pestle in liquid nitrogen. After

extraction, nuclei lysis, and sonication of chromatins, protein–DNA complexes were immunoprecipitated with GFP-trap Agrose beads from Proteintech (https://www.ptglab.com/). The precipitated DNAs were reverse-cross-linked and purified using a PCR Purification Kit (QIAGEN) and subjected to real-time quantitative polymerase chain reaction (Bio-Rad Laboratories) with primers targeting the *PIN1* promoter fragment and the control fragment in the *PIN1* coding region. Fold enrichment values were calculated based on Ct values between the *GFP-HVA* transgenic line and the control.

### Confocal microcopy and quantification of fluorescence signals

The reporter lines of *ProDR5::YFP*, *ProAtHB8::YFP* (Marquès-Bueno *et al.*, 2016) and *PIN1:PIN1-GFP* (Benková *et al.*, 2003) lines have been reported earlier. Stem cross sections at a thickness of 100 μm were freshly prepared from the reporter lines using a Leica Vibratome (Leica). For GFP signals, a Leica SP8 confocal microscope was used with consistent settings: excitation laser lines 488 nm, emission 580 nm, and scan speed 400 Hz. For YFP signals, A Nikon A1 plus confocal microscope was used with the following setting: excitation 513 nm, emission 632.5 nm, and a pinhole size of 42.15. The fluorescence signals were quantified using the ImageJ software (https://imagej.net/). In brief, individual vascular bundles showing fluorescence signals were selected with the freeform drawing tool. From the analyze menu, select 'set measurements' with 'area integrated intensity' and 'mean grey value' checked. The fluorescence signal then can be measured with the 'Measure' function from the analyze menu. Repeat these steps to measure fluorescence for all samples from different genotypes.

### Accession numbers

The accession nos. are as follows: HVA- AT5G27880; TOPLESS (TPL)-AT1g15750; SIN3 ASSOCIATED POLYPEPTIDE 18 (SAP18)-AT2G45640; ATHB8- AT4G32880; ALTERED PHLOEM DEVELOPMENT (APL)- AT1G79430; PIN-FORMED1 (PIN1)- AT1G73590.

## Results

### Identification of a mutant with increased bundle number in *Arabidopsis*

To identify novel regulators of vascular development, we screened an Arabidopsis activation-tagging mutant population using UV microscopy (Du *et al.*, 2015). A semi-dominant mutant showing high vascular activity, named *hva-d*, was identified from the screening. In WT plants, eight discrete clusters of protoxylem cells developed along the periphery of the stem in the tip region (Fig. 1a,b,j). Each protoxylem cluster, stained to a bright-red color by phloroglucinol, represents a vascular bundle as shown in toluidine blue staining (Fig. 2). The heterozygous *hva-d*/+ mutants developed *c.* 20 vascular clusters (Fig. 1e,j), while the homozygous *hva-d* mutants developed over 50 clusters (Fig. 1h,j). These results demonstrate that *hva-d* mutant plants develop an increased number of vascular bundles in the stem. In the middle stem regions, interfascicular fibers develop between vascular bundles, forming a continuous ring of lignified cells (Fig. 1c). An increased number of bundles were observed along the stem periphery, as well as in the center pith region in heterozygous (*hva-d*/+) and homozygous (*hva-d*) plants (Fig. 1f,i). At the bottom of the stem, WT plants showed increased xylem layers due to secondary growth (Fig. 1d). More layers of xylem cells were developed in *hva-d*/+ and *hva-d* plants, indicating increased secondary growth at the base of the stem (Fig. 1g,i). In addition, gaps formed in the ring of lignified cells due to lacking secondary cell wall formation in some regions in the *hva-d*/+ and *hva-d* mutant lines (Fig. 1g,i). Plant growth was negatively affected in mutant lines, which were noticeably smaller than the WT plants (Fig. S1). The *hva-d* homozygous mutant plants grew extremely short stems and barely bore any seeds (Fig. S1).

We further examined vascular development using toluidine blue staining. In WT stems, cell proliferation in procambium creates collateral bundles, in which the xylem forms toward the pith and the phloem forms toward the outside. Compared with the WT, cell proliferation was enhanced in the *hva-d* mutants, as shown by increased procambium (Fig. 2a,c,e,g), and interfascicular cambium regions in mature stems (Fig. 2b,d,f,h). The *hva-d*/+ and *hva-d* mutant lines also showed increased cambial cell number than WT plants (Fig. 2i). In addition, the *hva-d*/+ and *hva-d* plants develop lignified xylem cells in pith regions (Fig. 2c–f). These results indicated that the *hva-d* mutant plants showed increased vascular bundle number and enhanced cambium activity.

### Expression of vascular development reporters in the *hva-d* mutant

The *AtHB8* gene is specifically expressed in procambium precursor and procambial cells and serves as a marker for provascular development (Baima *et al.*, 1995; Donner *et al.*, 2009; Smetana *et al.*, 2019). To investigate cambium activity and vascular development, we compared the expression pattern of two *AtHB8* reporters between WT and *hva-d* mutant plants. First, the *ProAtHB8::GUS* reporter was investigated using GUS staining (Fig. 3a–c). In WT background, GUS activity was primarily detected in the (pro-)cambium of the vascular bundles (Fig. 3a). Intriguingly, high-intensity GUS staining was detected not only in (pro-)cambial regions but also in protoxylem and pith regions in the *hva-d*/+ plants (Fig. 3b). The *hva-d* plants showed the strongest GUS staining across the whole stem cross section, including the center pith region (Fig. 3c). These results indicated that provascular activity was significantly increased in the *hva-d* mutant lines. To confirm the GUS staining results, we examined another fluorescence reporter, a *ProAtHB8::YFP* line (Fig. 3d–j). In the WT background, the fluorescence was observed in the (pro-)cambium region, similar to the GUS staining (Fig. 3d–f). A weak YFP signal was observed in the protoxylem region in WT plants, indicating that the fluorescence reporter line is more

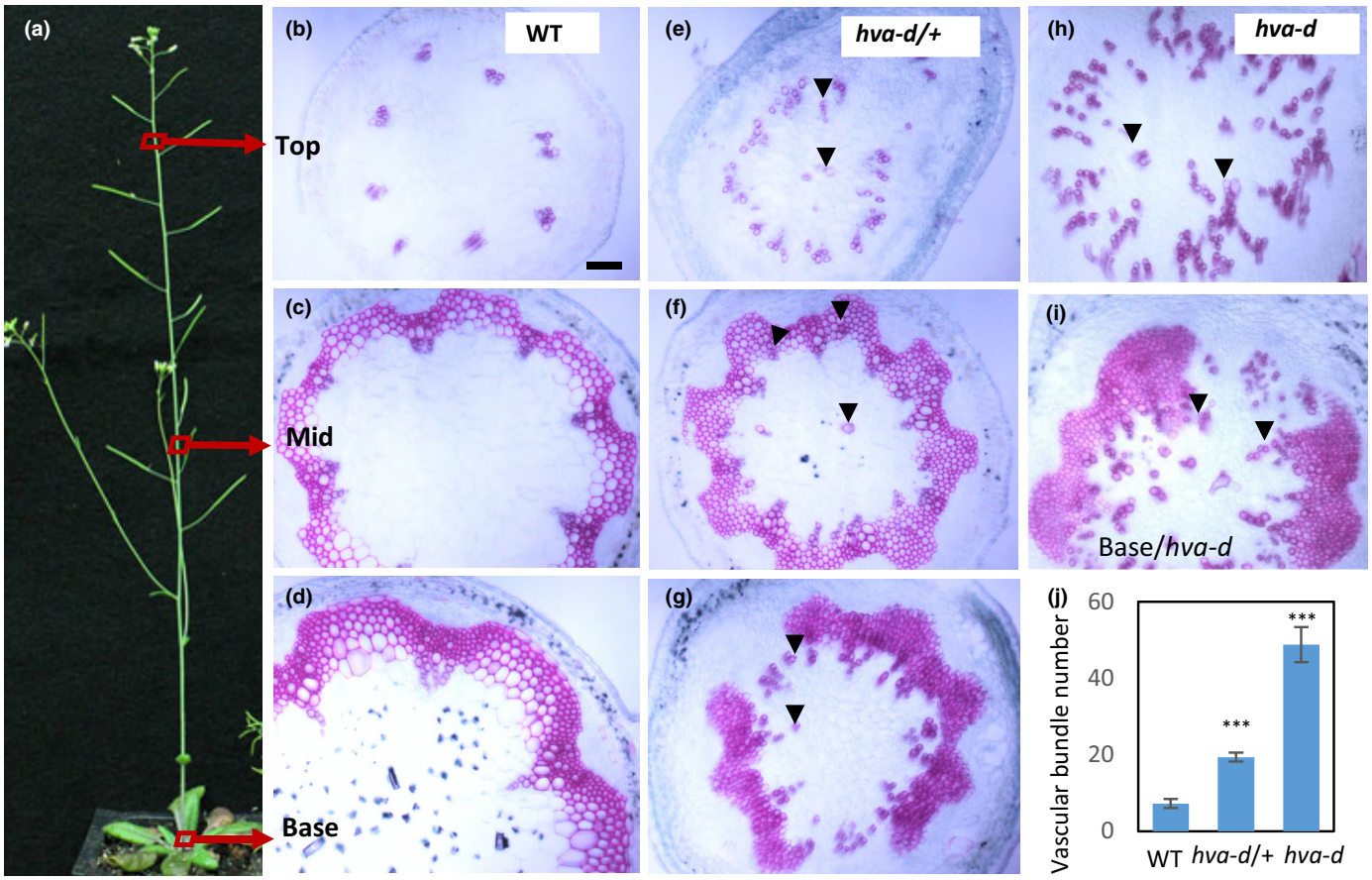


**Fig. 1** Increased vascular bundle number in *hva-d* mutant plants. (a) A wild-type (WT) plant used to demonstrate sectioning position. (b–d) Phloroglucinol staining of stem cross sections from the top (b), middle (c), and base of WT plants (d). Bar, 50 μm. (e–i) Phloroglucinol staining of stem sections of *hva-d*/+ heterozygous (e–g) and *hva-d* homozygous plants (h, i). Noting increased bundle number and ectopic vessels in the pith of the top of the stem (e, h), and the cross section from the base of the homozygous plant in (i). (j) Quantification of bundle numbers in the three genotypes using cross sections from the top of the stem. Only protoxylem clusters developed along the stem periphery were counted as a bundle. Values are means for ≥ 10 plants of respective genotypes. *** indicates statistically significant differences compared with WT by Student's *t*-test, $P < 0.0001$. Error bars represent ±SD.

sensitive than the GUS reporter (Fig. 3d–f). In the *hva-d*/+ plants, the YFP signal was observed in the procambium, as well as in the protoxylem and pith region similar to the *ProAtHB8::GUS* reporter results (Fig. 3g–i). Quantification of the fluorescence signal indicated a stronger expression of *ProAtHB8:YFP* in *hva-d*/+ plants (Fig. 3j). These results indicate that provascular development is enhanced in the *hva-d* mutant plants, consistent with the increased vascular bundle in the mutant lines.

To further characterize vascular development, we examined the expression of a phloem development marker *ProAPL::GUS* (Fig. S2). The *Altered Phloem Development* (*APL*) gene is specifically expressed in phloem tissues, including protophloem, companion cells, and metaphloem sieve elements. In WT plants, *GUS* activity was detected in the phloem of the young shoot tip (Fig. S2a). GUS activity was also observed in the interfascicular secondary phloem regions at the bottom of the stem (Fig. S2b). In the *hva-d*/+ mutant plants, GUS signals were diffused in the young stem (Fig. S2c) and became more intense in the mature region at the stem bottom (Fig. S2d). GUS signals were observed in a broad area in both young and mature stems in the *hva-d* mutant (Fig. S2e,f). Intriguingly, the GUS signal was observed only in the stem periphery, but not in the pith region (Fig. S2e, f). These results indicated that the *hva-d* plants develop relatively normal phloem despite the enhanced provascular activity.

## Activation of *AT5G27880* is responsible for the *hva-d* mutant phenotypes

To identify the gene(s) causing the *hva-d* mutant phenotype, we performed a plasmid rescue experiment to determine the insertion locus of the activation tag (Weigel *et al.*, 2000). Sequencing of the rescued plasmid indicated that the insertion is 2.4 kb upstream of *AT5G27889* and 11.7 kb downstream of *AT5G27880* on *Arabidopsis* chromosome 5 (Fig. 4a). To examine whether the activation tag cosegregates with the observed phenotypes, we genotyped a segregating T3 population. Among 224 T3 plants, we identified 55 WT plants, 122 heterozygous plants, and 47 homozygous plants. All heterozygous and homozygous plants displayed dwarf growth phenotype and increased vascular bundle number compared with WTs. The segregation ratio is

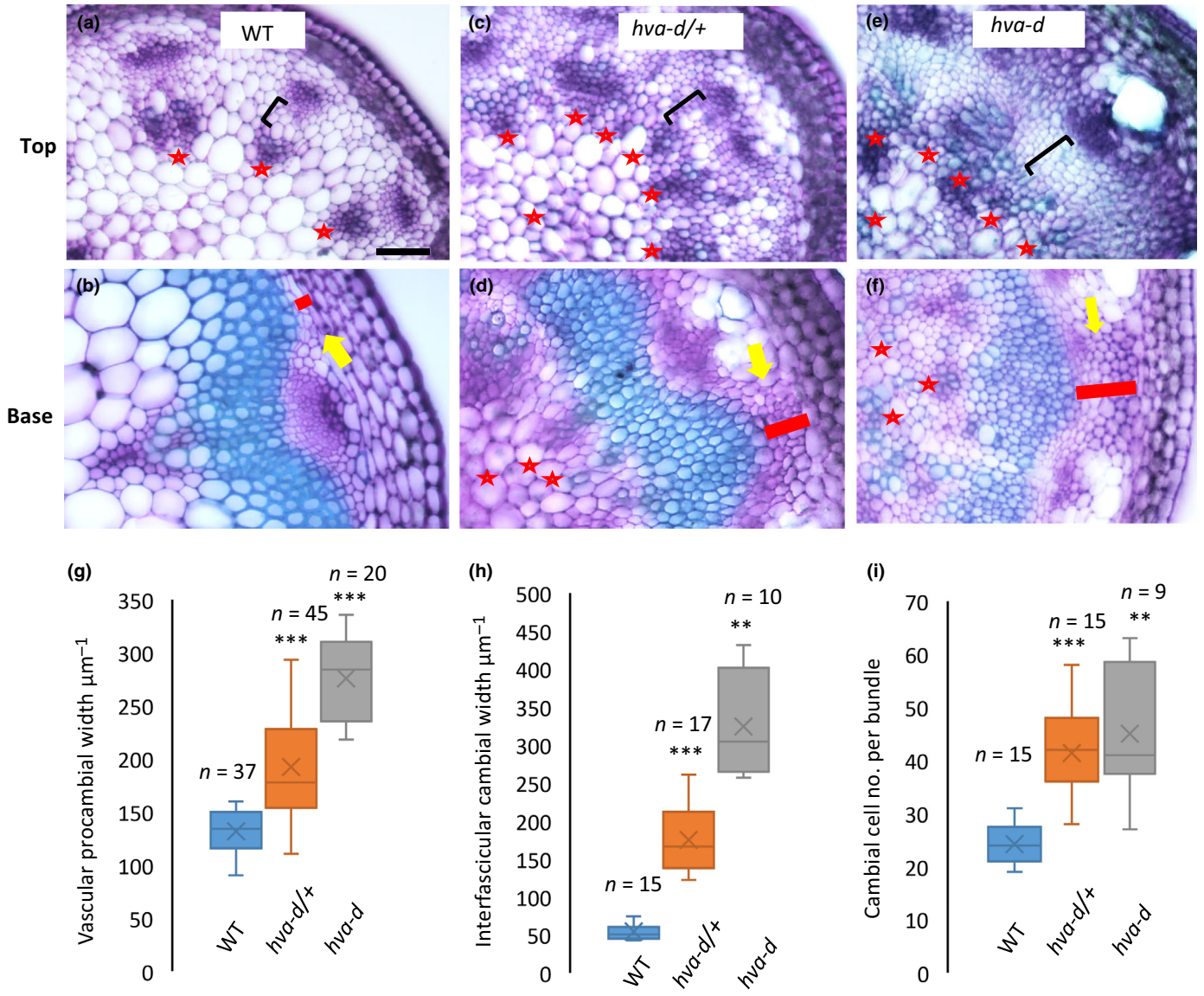


**Fig. 2** Enhanced cambium activity in the *hva-d* mutant plants. (a–f) Toluidine blue staining of stem cross sections of wild-type (WT) (a, b), *hva-d*/+ (c, d), and *hva-d* mutant plants (e, f). Black square brackets denote procambium region. Yellow arrows point to cambium regions showing increased layers of undifferentiated cells in mutant plants. Stars denote bundles (a–e). Red bars denote width of cambium region (b–f). Bar, 50 µm. (g) Quantification of vascular procambial width of the top stem sections in the three genotypes. (h, i) Quantification of the cambial width (h) and cell numbers per bundle (i) at the stem base in three genotypes. **, and *** indicate a statistically significant difference compared with WT control by Student's *t*-test, $P < 0.001$, and $P < 0.0001$, respectively. Whisker lines indicate variability outside the upper and lower quartiles (g–i).

consistent with single gene inheritance with an expected 1 : 2 : 1 ratio ($\chi^2 = 2.57$, $P = 0.308$). These results suggested that the vascular defects and dwarfism phenotypes are due to this single activation tag insertion.

We then examined the expression of all three genes in a 15 kb range, both up and downstream of the activation tag insertion. All genes were highly upregulated in *hva-d* mutant compared with the WT (Fig. 4b). Therefore, we reasoned that one of the three genes might be responsible for the *hva-d* phenotypes. We first overexpressed *AT5G27880*, encoding a C2H2 transcription factor. The overexpression construct used the 4 × 35S enhancer to drive the expression of a genomic region of *AT5G27880*, including a 1038 bp promoter and a 600 bp sequence downstream of the coding region. Thirty-five of 38 transgenic plants displayed growth phenotypes similar to the *hva-d* mutant. Among these 35 transgenic plants, 11 exhibited extremely severe growth defects with no elongated stems. Two of the transgenic lines, *AT5G27880-OX1* and *AT5G27880*-OX5, were analyzed and confirmed overexpression of the *AT5G27880* gene (Fig. 4c, d). The transgenic plants showed an increased number of vascular bundles and ectopic protoxylem formation in the pith region (Fig. 4d). These results demonstrated that overexpression of *AT5G27880* resulted in *hva-d* phenotypes. The other two genes, *AT5G27889* and *AT5G27890*, were also overexpressed using the

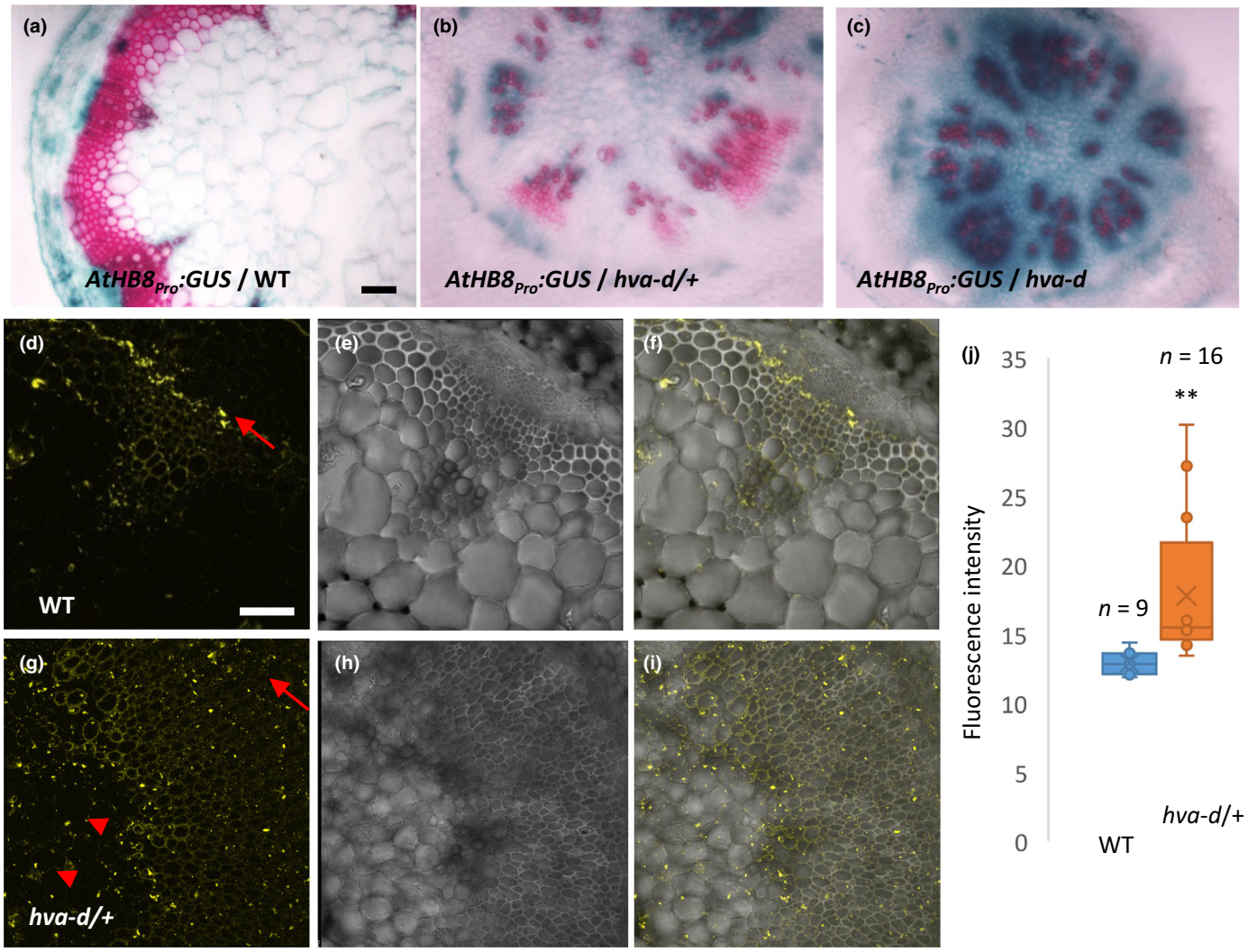


**Fig. 3** Characterization of prevascular reporters showing enhanced vascular formation in *hva-d* mutant lines. (a–c) Examination of prevascular marker *ProAtHB8:GUS* in wild-type (WT) (a), *hva-d/+* (b), and *hva*-d mutant plants (c). (d–j) Characterization of prevascular activity using the *proAtHB8::YFP* reporter. (d–i) Fluorescent microscopy analysis of *proAtHB8::YFP* reporter at YFP channel (d, g), bright light (e, h), and overlay of the two channels (f, i). Bars, 50 μm. (j) Quantification of fluorescence signal intensity in WT and *hva-d/+* mutant plants. ** indicates statistically significant differences compared with WT by Student's *t*-test, $P < 0.001$. Whisker lines indicate variability outside the upper and lower quartiles. Arrows indicate YFP signals from the cambium region. Arrow heads denote YFP signals in pith region. All images were taken with identical settings.

same overexpression vector. A 5.5 kb genomic sequence including a 2.7 kb 5′ region, coding sequences of *AT5G27889* and *AT5G27890*, and a 0.9 kb downstream region were inserted after the 4 × 35S enhancers and transformed into WT plants. After screening on antibiotic supplied plates, 72 resistant plants were transferred to soil, but none showed similar growth phenotypes as *hva-d* mutant. We randomly selected nine plants for cross section and found normal vascular organizations as WT plants (Fig. S3). These results indicate that *AT5G27880* is the causal gene of the *hva-d* mutant phenotypes.

To further investigate the function of *AT5G27880*, we designed an artificial microRNA to silence its expression in the *hva-d* mutant (Schwab *et al.*, 2006). Three independent transgenic lines, *miRNA-4*, *miRNA-8*, and *miRNA-10*, were selected for further analyses. Quantitative reverse transcription polymerase chain reaction assay indicated that the transcripts level of *AT5G27880* was significantly repressed in these transgenic lines compared with *hva-d/+* plants (Fig. 4e,f). Accordingly, both plant height and stem vascular patterns were restored to WT (Fig. 4f,g). These experiments further demonstrate that overexpression of *AT5G27880* is responsible for the *hva-d* phenotype. We therefore renamed *AT5G27880* as *HVA*.

## HVA is a nucleus-localized transcriptional repressor

The *HVA* gene encodes a putative transcription factor in the $C_2H_2$ zinc finger superfamily that comprises 176 members in *Arabidopsis* (Englbrecht *et al.*, 2004). Multiple sequence alignment of the closely related proteins revealed high similarity between their conserved $C_2H_2$ domains and C-terminal EAR

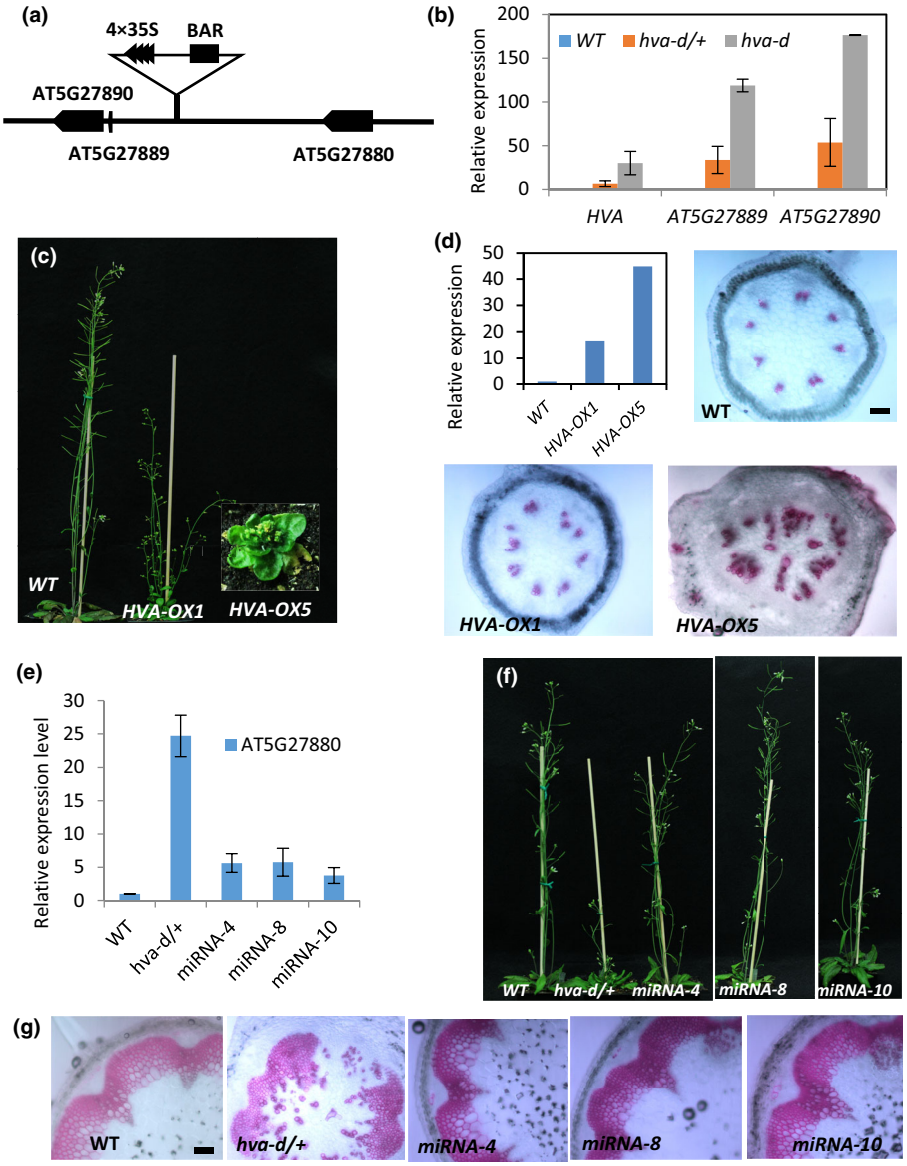


**Fig. 4** Activation of AT5G27880 (HVA) is responsible for the *hva-d* mutant phenotype. (a) Schematic diagram of the genomic region flanking the T-DNA insertion site. (b) The *AT5G27880*, *AT5G27889*, and *AT5G27890* genes are upregulated in the *hva-d* mutants. Values are means ±SD of three biological replicates. *UBQ5* is used as the reference gene. (c) Transgenic plants overexpressing *AT5G27880* (hereafter HVA) mimicked *hva-d* mutant in plant growth. (d) Overexpression of *HVA* increases bundle number in two *trans*genic lines, *HVA-OX1* and *HVA-OX5*. Cross sections of the two transgenic lines showed more vascular bundles and ectopic xylem cells in pith similar to *hva-d* mutant. (e) Expression of *HVA* is repressed in the artificial microRNA (miRNA) transgenic plants compared to *hva-d/+* plants. Values are means ±SD of three biological replicates. *UBQ5* is used as the reference gene. (f) Knocking down *HVA* expression restored the plant growth of the *hva-d/+* mutant to WT. (g) Vascular defects were recovered to WT in the miRNA transgenic plants. Bar, 50 μm.

motif (Fig. S4). The EAR motif has been shown to have transcriptional repression activity in a broad range of developmental and physiological processes (Ohta *et al.*, 2001).

To investigate the subcellular localization of HVA, a green fluorescent protein (eGFP) was fused to the N terminus of HVA (*eGFP-HVA*). The construct driven by a CaMV 35S promoter was transformed into WT plants. GFP signal was detected in the nucleus of root hair cells, consistent with the role of HVA as a transcription factor (Fig. 5a). Nuclear localization of eGFP-HVA was also observed in other cell types in the root (Fig. S5a,b). To characterize the expression pattern of *HVA* gene, we performed a transgenic experiment using the *ProHVA::GUS* construct (Fig. S5c–g). GUS staining indicated that *HVA* expression was detected in flower, leaf, siliques, and young stems. We did not detect GUS signals in roots from the seedling stage (Fig. S5g). In the stem cross sections, the GUS signal was strong in vascular bundles, especially in the phloem region and on the phloem side of the cambium (Fig. 5b,c). This result is consistent with a previous transcriptome profiling study showing HVA expression in the stem and relatively high expression in the phloem side of the vascular cambium (Fig. S5h). Real-time PCR analysis of mature plant tissues indicated that *HVA* is relativelyhighly expressed in roots, leaves, and young stems (Fig. S5i). The expression of *HVA* is consistent with its function in vascular development.

The C-terminus of HVA protein has an EAR motif featured by an LSLSL amino sequence (Fig. S4). We performed a transient expression assay to determine whether HVA has a repressor function. This assay involves cotransforming reporter constructs and effector constructs into Arabidopsis protoplast (Fig. 5d). The reporter construct includes a firefly luciferase gene (*LUC*) driven by a minimal 35S promoter followed by five copies of the GAL4-binding site and a TATA box (Fig. 5d). The effector constructs express a protein of interest fused with a yeast GAL4 DNA-binding domain (GAL4-DB) (Fig. 5d). In this assay, HVA and two HVA mutations, truncation of EAR domain (HVA NO

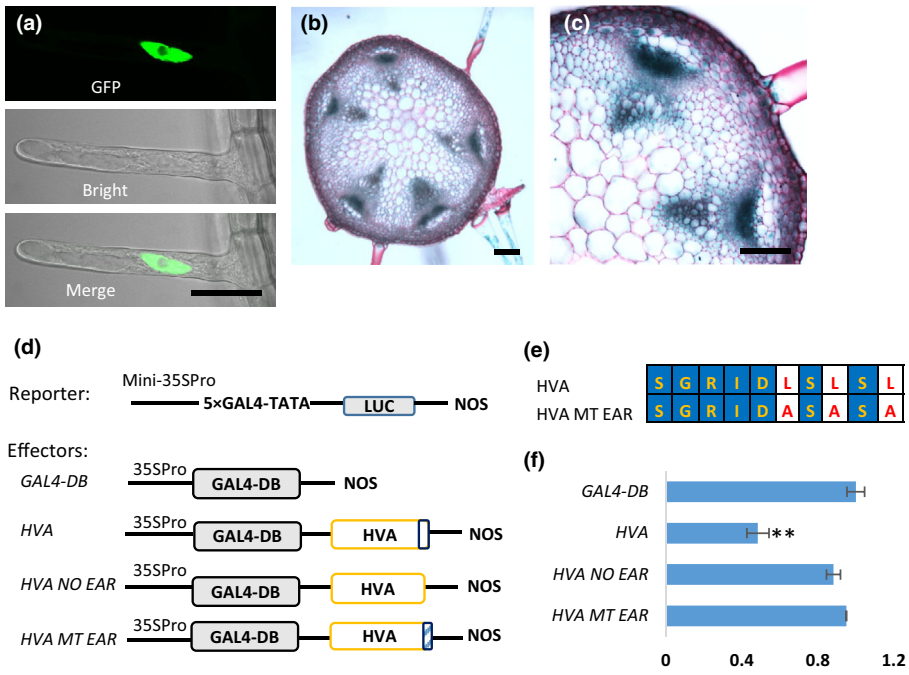


**Fig. 5** High Vascular meristem Activity (HVA) is localized in the nucleus and functions as a transcriptional repressor in vascular tissues. (a) Confocal images showing HVA localization in nucleus of 5-d-old lateral root cells. Bar, 20 μm. (b, c) GUS staining showing expression of *ProHVA::GUS* in stem tissues. Bars, 50 μm. (d) Constructs used in transactivation assay. HVA has an Ethylene-responsive element binding factor-associated Amphiphilic Repression (EAR) domain (LSLSL) in the C-terminus. (e) Amino acid sequence of the EAR domain in HVA and the mutated EAR domain (HVA MT EAR). The mutations are labeled in red. (f) Relative transaction activities of different Effectors. GAL4-DB was used as a control. ** indicates statistically significant difference compared with control by Student's *t*-test, $P < 0.001$. Error bars represent ±SD of three biological replicates.

EAR), and lysine to alanine mutations (HVA MT EAR), as well as the GAL4-DB control were analyzed for repression function (Fig. 5d,e). Bioluminescence measurements revealed that luciferase activity was reduced by > 50% in the presence of full-length HVA, while deletion or mutation of the EAR motif showed similar luciferase activity as the vector control (Fig. 5f). These results indicated that HVA is a transcriptional repressor, and the repression depends on a functional EAR domain.

To further confirm the importance of the EAR motif for the biological function of HVA, we overexpressed HVA without the EAR motif (*HVAΔEAR*) under the control of a 4 × 35S enhancer in *Arabidopsis* WT. As a result, three transgenic plants (*HVAΔEAR-OX6*, *8*, *17*) showed overexpression of the truncated *HVA*, but none of the lines exhibited phenotypes as the *hva-d* mutant (Fig. S6). Therefore, HVA is a nucleus-localized transcriptional repressor, and the EAR motif is essential to its biological function.

## Interaction with TPL is required for HVA biological function

The EAR domain presents in many transcription factors, such as WUS, IAA12, BES1, and BZR1, all of which play essential roles in plant development. Physical interaction between the EAR motif and corepressor TPL or SAP18 has been reported in *Arabidopsis* (Szemenyei *et al.*, 2008; Kagale & Rozwadowski, 2011). Because HVA protein is repressor with the conserved EAR motif (LSLSL), we reasoned that it might also directly interact with corepressors, such as TPL or SAP18. Therefore, we performed a protein interaction assay using a pairwise yeast two-hybrid assay. First, we confirmed that HVA directly interacts with TPL (Fig. 6a). The interaction depended on the EAR motif, because deletion of the EAR motif abolished protein interactions in yeast (Fig. 6a). Using the same approach, we detected no interaction between HVA and SAP18 in yeast (Fig. S7).

To confirm the close association between HVA and TPL *in planta*, we performed a BiFC assay in *N. benthamiana* leaves. Fluorescence of the reconstituted split YFP protein was observed in the nucleus of leaf cells cotransfected with the HVA-N-YFP and TPL-C-YFP constructs, indicating a possible direct interaction between HVA and TPL (Fig. 6b, upper panels). Further analysis indicated the EAR domain was necessary for the interaction between HVA and TPL because no YFP fluorescence could be observed in cells co-expressing HVAΔEAR-N-YFP and TPL-C-YFP (Fig. 6b, lower panels). These results demonstrated that HVA interacts with TPL through the EAR domain.

The interaction between HVA and TPL indicates that TPL may be involved in vascular bundle formation. To investigate the biological function of TPL, we performed genetics analyses using TPL loss-of-function mutant lines. Because the *tpl-1* mutant is seedling lethal and could not be used for genetic analysis, we employed a transgenic approach instead. The mutation from asparagine to histidine at the position of 176 (N176H) in the TPL protein (mtTPL) resulted in a dominant-negative effect in the *tpl-1* mutant (Long *et al.*, 2006; Osmont & Hardtke, 2008). In this study, we transformed an *mtTPL* (N176H) construct driven by *UBQ10* promoter into the *hva-d*/+ plants. After antibiotic screening and genotyping, we obtained 18 *UBQ10::mtTPL* transgenic plants in *hva-d*/+ background. The plant growth of nine of the 18 transgenic plants was partially complemented (Fig. 6c). Stem cross section and histochemical analyses indicated that vascular bundle number was recovered to the level of WT plants, while silique development was not fully recovered (Fig. 6d). The partial complementation might be because the *UBQ10* promoter expression domain does not totally overlap with HVA gene activation. The results from biochemical analyses and transgenic studies indicate that TPL protein is required for HVA function in plant growth and vascular development.

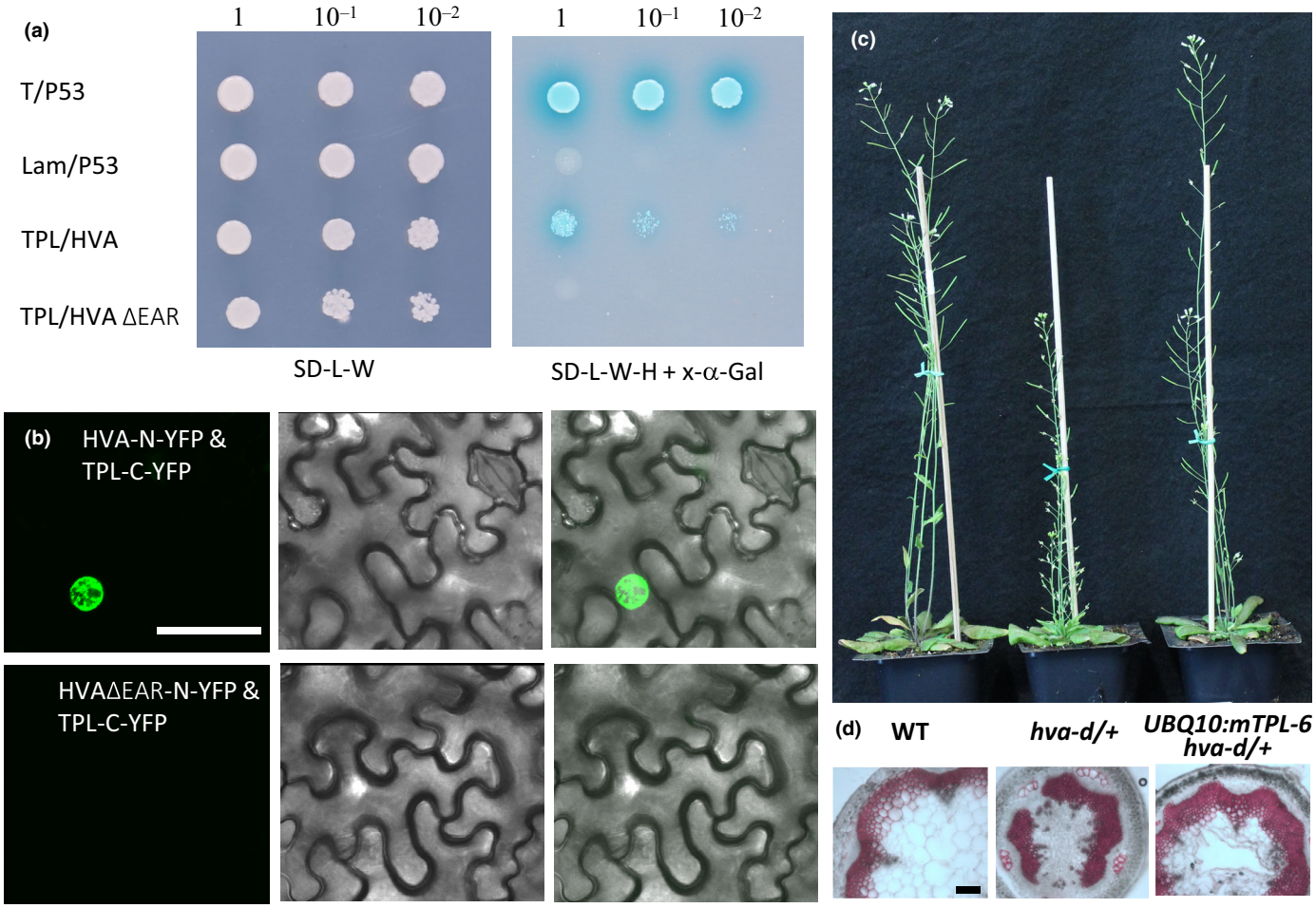


**Fig. 6** Interaction with TOPLESS (TPL) is required for High Vascular meristem Activity (HVA) biological function. (a) Yeast two-hybrid experiment showing HVA interacts with TPL. Noting that HVA with the deletion of Ethylene-responsive element binding factor-associated Amphiphilic Repression (EAR) domain (HVAΔEAR) does not interact with TPL. The positive control is the interaction between p53 and T-antigen, and the negative control is the co-transformation of Lamin C and T-antigen. (b) Bimolecular fluorescence complementation analysis showing an interaction between HVA and TPL in *Nicotiana benthamiana* leaves. Upper panels showing cotransformation of *N*-YFP-HVA and *C*-YFP-TPL at YFP channel (left), bright light (middle), and overlay (right). Lower panels showing cotransformation of *N*-YFP-HVAΔEAR and *C*-YFP-TPL at the YFP channel (left), bright light (middle), and overlay (right). Bar, 50 μm. (c, d) Repression of TPL function restores plant growth and stem phenotypes of *hva-d* to wild-type (WT). Plant growth of 35-d-old WT, *hva-d*/+, and a transgenic plant harboring a *UBQ10:mTPL* construct (c). Phloroglucinol staining of stem cross sections of WT, *hva-d*/+, and a transgenic plant expressing *UBQ10:mtTPL*. Bar, 100 μm (d).

## Knockout of *HVA* using a CRISPR-Cas approach or expressing *HVA-VP16* resulted in fewer vascular bundles

There are no available mutant lines that either knock out or knock down the expression of *HVA* in stock centers (https://www.arabidopsis.org/). To investigate whether mutation of HVA reduces bundle number in Arabidopsis stem, we generated *hva* knockout mutants using a CRISPR-cas9 approach (Stuttmann *et al.*, 2021). We designed two sgRNAs targeting the *HVA* gene with the intention of causing substantial deletions (Fig. S8a). Indeed, two *hva* knockout mutant lines, *hvacr-7* and *hvacr-29*, resulted in large deletions in the *HVA* gene (Fig. S8a). While the full-length *HVA* is expressed in WT plants, only truncated transcripts of *HVA* were detected from the gene-edited lines (Fig. S8b). A significant reduction in vascular bundle number was observed in the two knockout mutant lines, as shown by phloroglucinol staining of cross sections prepared from the middle and the bottom of the stem (Fig. 7a) and quantification analysis (Fig. 7b). The two knockout *hvacr* mutant lines are slightly shorter than the WT and otherwise relatively normal in other organ development (Fig. S8c). Toluidine blue staining also showed a reduction in vascular bundles and a relatively normal vascular pattern in the two *hva* knockout CRISPR lines (Fig. S8d–f).

The EAR domain of HVA protein is critical in affecting vascular bundle formation (Fig. 6). Therefore, we reasoned that replacing the EAR domain with an activation domain should change the functionality of HVA. To investigate this possibility, we generated a construct by removing the EAR domain of HVA, and replacing it with a VP16 domain, which has a potent activation function (Seipel *et al.*, 1994; Shih *et al.*, 2014). The *HVA-VP16* construct was transformed into WT plants. Thirty-six transgenic

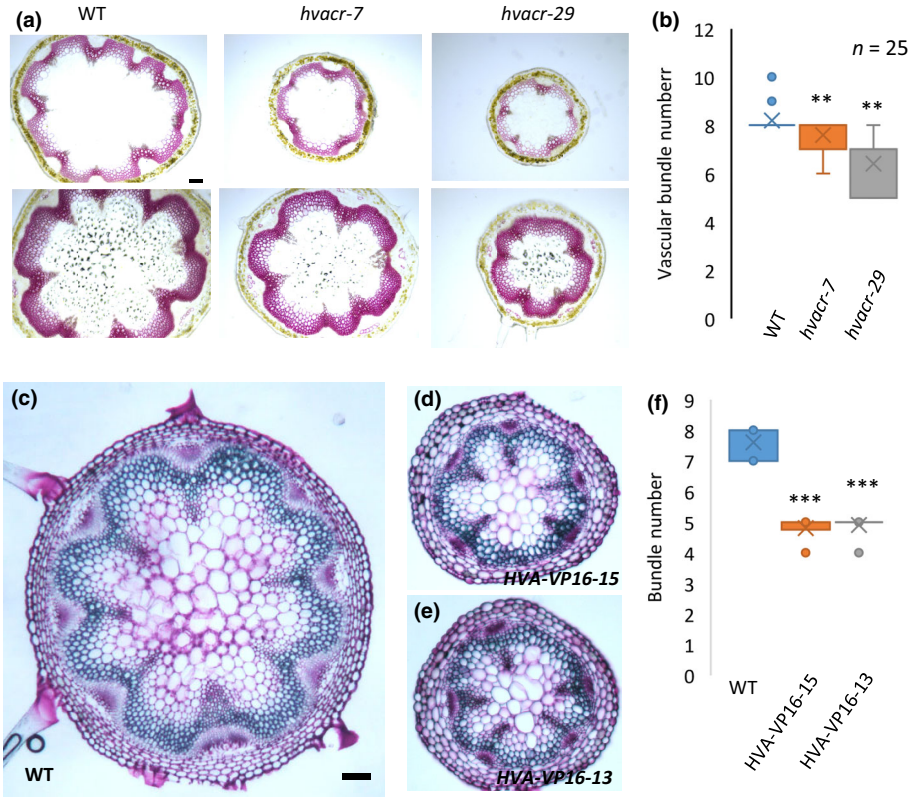


**Fig. 7** Knockout of High Vascular meristem Activity (HVA) or expression of an HVA-VP16 fusion construct reduces bundle number. (a) Phloroglucinol staining of stem cross sections at the middle (upper panels) and bottom (lower panels) from wild-type (WT) and the two CRISPR lines, *hvacr-7* and *hvacr-29*. Bar, 100 μm. (b) Quantification of vascular bundle numbers of the two mutant lines. ** indicates a significant difference, two-tailed Student's *t*-test, $P < 0.001$. (c–e) Toluidine blue staining of stem cross sections of a WT plant (c), transgenic line *HVA-VP16-15* (d), and *HVA-VP16-13* (e). Bar, 100 μm. (f) Quantification of bundle numbers in WT and two transgenic lines, $n = 10$. *** indicates statistically significant difference compared with WT control by Student's *t*-test, $P < 0.0001$. Whisker lines indicate variability outside the upper and lower quartiles.

plants were identified and showed distinct phenotypes of dwarfism, narrow leaves, and thin stems (Fig. S9a). Expression of *HVA-VP16* was confirmed with quantitative reverse transcription polymerase chain reaction (Fig. S9b). The transgenic lines developed fewer vascular bundles than WT plants, as shown by results from stem cross sections and quantification analysis (Fig. 7c–f). The increased bundles in *HVA* activation-tagging lines and reduced bundles in HVA knockout and HVA-VP16 fusion transgenic lines indicate that HVA positively regulates vascular bundle formation. Because the *HVA-VP16* transgenic lines showed strong and consistent phenotypes, we used the *HVA-VP16-15* transgenic line for further analyses.

## HVA regulates vascular formation through the auxin efflux facilitator PIN1

To understand the regulatory mechanism of HVA in controlling vascular bundle development, we performed a transcriptome analysis using a microarray approach. As expected, genes around the activation tag, including *HVA*, *AT5G27889*, and *AT5G27890*, are all highly overexpressed, indicating that the transcriptomic data are reliable (Table S2). Because HVA functions as a transcriptional repressor and the EAR domain is essential to the *hva-d* phenotypes (Fig. 6), we focused on those downregulated genes in *hva-d* for identifying candidate genes function downstream of HVA in regulating bundle number. Among the 121 downregulated genes (> 2 folds), we found genes involved in vascular development, for example *LBD1* (Ye *et al.*, 2021), *KAN3* (Ilegems *et al.*, 2010); cell wall biosynthesis, for example Cinnamyl Alcohol Dehydrogenase 5 (*CAD5*) and Wall-Associated receptor Kinase 3 (*WAK3*); and genes in stem elongation, for example *Expansin* 23 (*EXPA*23), *EXPA*25, and *EXPA16* (Table S2). These genes play roles in vascular development but may not be responsible for initiating bundles and determining bundle numbers in stems.

Previous analyses have found that auxin transport and brassinosteroids (BR) signaling/synthesis are negative and positive regulators of vascular bundle number, respectively (Ibañes *et al.*, 2009). By contrast, auxin levels do not alter the number or arrangement of vascular bundle number (Ibañes *et al.*, 2009). Because HVA is a transcriptional repressor, we focused on genes influencing auxin transport in the downregulated genes. Among all auxin efflux facilitator genes, *PIN*1-7, only *PIN1* is slightly downregulated (−1.3 fold) in the *hva-d* mutant in our microarray analysis (Table S2). To confirm the results from the transcriptome analysis, we checked the expression of *PIN1* in both the *hva-d* mutant and the *HVA-VP16* transgenic plants using quantitative reverse transcription polymerase chain reaction. The results clearly showed that the *PIN1* transcript level was significantly downregulated in the *hva-d* mutant, and upregulated in the *HVA-VP16* transgenic plants (Fig. 8a,b), indicating that HVA potentially represses *PIN1* expression in the stem.

To further investigate whether HVA affects *PIN1* expression, we performed a dual-luciferase assay (Fig. 8c). In this assay, the function of HVA was analyzed by cotransforming a HVA effector with a reporter construct, in which the *PIN1* promoter drives the Firefly luciferase gene expression. Compared with the control (CK), cotransformation of the *HVA* effector significantly

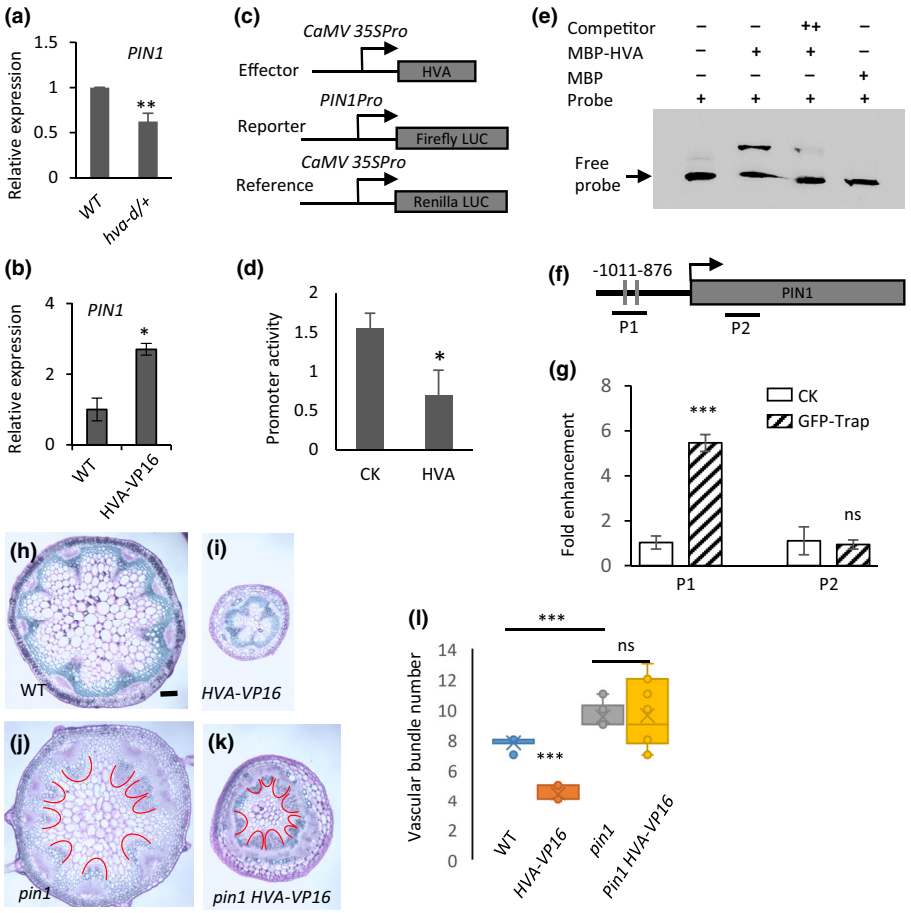


**Fig. 8** High Vascular meristem Activity (HVA) directly regulates PINFORMED1 (PIN1) expression and vascular development. (a, b) Expression of *PIN1* in *hva-d* (a) mutant and *HVA-VP16* transgenic plants (b). Error bars represent ±SD of three biological replicates. (c) Diagrams showing constructs used for dual-luciferase assay. (d) Relative promoter activity of effector control (CK) and HVA effector showing repression of PIN1 promoter by HVA. The constructs of effectors, reporter, and reference were co-transformed, into leaf mesophyll cell protoplasts for luciferase activity assay. Error bars represent ±SD of three biological replicates. (e) Electrophoretic mobility shift assay showing direct binding of HVA to a fragment of the *PIN1* promoter. Noting unlabeled competitor abolishes shifted band, confirming binding specificity. (f) Schematic diagram of the *PIN1* gene structure including the promoter. Predicted C2H2 binding motifs (AATGAT) were labeled as vertical lines. Two fragments, P1 and P2, are used for qRT-PCR analyses. (g) ChIP-qPCR analysis showing the enhancement of P1 fragment indicating HVA binding to P1 *in vivo*. Error bars denote SE from three biological replicates. (h–k) Toluidine blue staining of stem cross sections of wild-type (WT) (h), plants expressing *HVA-VP16* (i), *pin1* mutant (j), and *pin1 HVA-VP16* double mutant (k). Bundles are marked with stars. (l) Quantification of vascular bundle numbers from four genotypes, $n = 10$. *, **, and *** indicates statistically significant differences compared with WT or CK by Student's *t*-test, $P < 0.05$, $P < 0.001$, and $P < 0.0001$. Whisker lines indicate variability outside the upper and lower quartiles. ns, no significant differences.

decreased the *PIN1* promoter activity (Fig. 8c), indicating that HVA may regulate *PIN1* expression through the *PIN1* promoter. To investigate whether HVA directly binds to the *PIN1* promoter, we performed an electrophoretic mobility shift assay (EMSA). The HVA protein was fused with a maltose-binding protein (MBP) and heterologously expressed in *E. coli* cells. Compared with the MBP control, adding HVA protein shifted the mobility of a biotin-labeled probe, a fragment of the *PIN1* promoter containing two putative $C_2H_2$ protein binding sites (Fig. 8d). The shifted band was significantly reduced by adding competing unlabeled DNA fragments, suggesting the specificity of the binding between the HVA protein and the probe (Fig. 8d). The EMSA experiment demonstrated that HVA binds to the promoter and regulates *PIN1* gene expression. To investigate whether HVA bind to PIN1 promoter *in vivo*, we performed a ChIP-qPCR analysis. We generated a transgenic line by transforming the *Pro35S::GFP-HVA* construct into *hvacr-29*. The transgenic plants showed the same number of bundles as the WT and were used for ChIP experiment. Quantative PCR analysis indicated that HVA directly bind to the *PIN1* promoter as shown by a sixfold enhancement of the promoter DNA fragment compared with the control fragment in the *PIN1* conding region (Fig. 8f,g). The ChIP-qPCR experiment further confirmed that HVA directly regulated the expression of *PIN1* gene.

To investigate whether HVA regulates vascular development through PIN1 *in planta*, we crossed an *HVA-VP16* transgenic line with the *pin1* mutant (SALK_047613). The *pin1* mutant showed the classic pin-shaped shoot structure (Figs 8, S10a). The double mutant was confirmed with expression analysis using reverse transcription polymerase chain reaction and a PCR-based

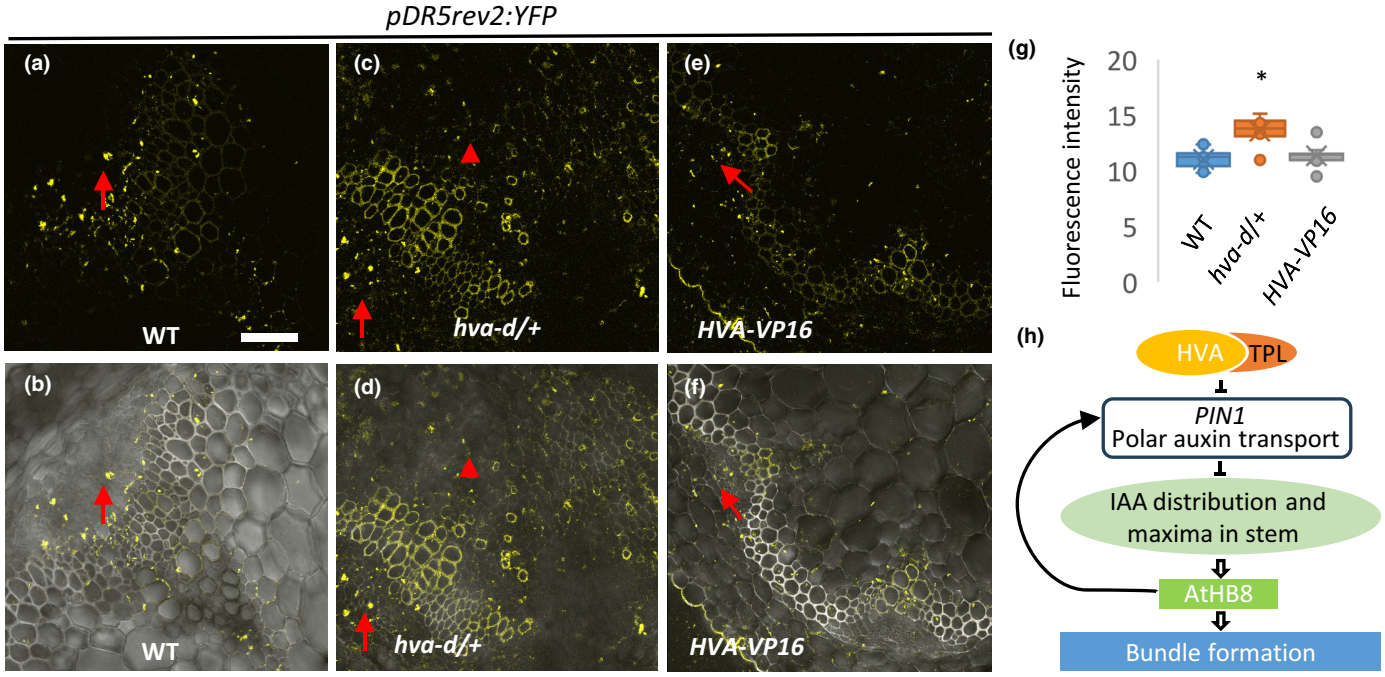


**Fig. 9** Characterization of auxin distribution using the *ProDR5::YFP* reporter. (a–f) Fluorescent microscopy analysis of *ProDR5::YFP* reporter at YFP channel (a, c, e), and overlay of YFP with bright-light channel (b, d, f). (g) Quantification of fluorescence signal intensity in wild-type (WT), *hva-d/+*, and *HVA-VP16* transgenic plants. Bar, 50 μm. * indicates statistically significant differences compared with WT by Student's *t*-test, $P < 0.05$. Whisker lines indicate variability outside the upper and lower quartiles. Arrows indicate YFP signals from the cambium region, noting increased signal intensity in the *hva-d/+* mutant plants. Arrow heads indicate YFP signals in the pith region. All images were taken with identical settings. Signals from xylem regions are autofluorescence. (h) A functional model depicting the function of HVA.

genotyping experiment (Fig. S10b,c). Characterization of stem cross sections indicated that the double mutant developed similar numbers of vascular bundles as the *pin1* mutant plants (Fig. 8h–l). As previously reported, *pin1* mutant shows radial xylem proliferation in bundles (Gälweiler *et al.*, 1998). We also observed expansion of the xylem region in bundles of *pin1* and the *pin1 HVA-VP16* double mutant lines, confirming PIN1 functions downstream of HVA in vascular development (Fig. 8). The genetic analyses further confirmed that PIN1 is downstream of HVA in regulating vascular bundle number. To confirm whether HVA regulates *PIN1* expression *in planta*, we crossed a *PIN1:PIN1-GFP* reporter line into the *hva-d* mutantand the *HVA-VP16* transgenic line. Quantification of the fluorescence signal showed that fluorescence intensity decreased in *hva-d/+* plants (Fig. S11a,b). These results are consistent with the quantitative reverse transcription polymerase chain reaction analyses and indicate that HVA negatively regulates PIN1 function. Characterization of the longitudinal sections showed the typical polar localization of PIN1 protein in different backgrounds, and the wide spread of cells showing GFP signals in the *hva-d/+* mutant plants (Fig. S11c). These results indicate that HVA affects the expression of *PIN1* gene, but not polar localization of PIN1 protein.

Disruption of auxin transport often affects auxin distribution in the stem. Indeed, some genes coding auxin-responsive proteins, including eight SAUR-like proteins and six GH3 family proteins, which are upregulated in *hva-d/+* mutant compared with WT (> 1.3 folds, Table S2). To investigate whether auxin distribution are affected by *HVA*, we crossed the *hva-d/+* and *HVA-VP16* transgenic plants with an auxin reporter line *ProDR5::YFP* (Brackmann *et al.*, 2018). In WT plants, YFP signals were restricted mainly in the protoxylem regions and occasionally in the cambium and xylem parenchyma cells (Fig. 9a,b). By contrast, strong YFP signals were detected in the cambium, protoxylem, and pith region in the *hva-d/+* mutants, indicating enhanced local auxin contribution in the mutant stem (Fig. 9c, d). In the *HVA-VP16* transgenic plant, YFP signal was also restricted in the vascular cambium and xylem parenchyma cells (Fig. 9e,f). Quantification of fluorescence intensity indicated that the YFP signal is much stronger in the *hva-d/+* mutants (Fig. 9g). These results indicated that repressing *PIN1* expression in *hva-d/+* mutant affected auxin distribution, therefore enhancing vascular bundle formation.

Treatment with auxin transport inhibitor NPA is known to increase auxin content above the treatment zone in the stem (Suer *et al.*, 2011). We treated *HVA-VP16* transgenic plants with NPA to investigate whether the treatment can partially alleviate the cambium-related phenotypes. In *HVA-VP16* plants treated with NPA, the YFP signals spread to the cortex and interfascicular regions and intensified in the vascular bundle regions, indicating enhanced auxin accumulation (Fig. S12a,b). Characterization of the NPA-treated *HVA-VP16* plants showed increased cambial cell division, especially in the interfascicular regions (Fig. S12c,

d). The NPA treatment does not enhance vascular bundle number. We reasoned that vascular bundles are already formed at the time of NPA treatment and, therefore, are not affected by the treatment. These observations indicate that blocking auxin transport by NPA treatment enhances auxin accumulation and increases cambial activity in the *HVA-VP16* plants.

## Discussion

Three mutants showing high cambium activity have been reported previously, including *cov1* (Parker *et al.*, 2003), *hca* (Pineau *et al.*, 2005), and *hca2* (Guo *et al.*, 2009). The *cov1* and *hca* mutants are recessive alleles derived from EMS mutagenesis and T-DNA insertion, respectively. The activation-tagging line *hca2* showed increased interfascicular cambium activity without altering the organization of vascular bundles in stems (Guo *et al.*, 2009). In this paper, we report a novel activation-tagging mutant, *hva-d*, with an increased vascular bundle number and enhanced vascular cambium activity. Unlike the previously reported mutants only affecting cambium activity, the *hva-d* mutant showed unique phenotypes in vascular bundle number and patterning. Histochemical analysis indicates that protoxylem formation was highly activated in *hva-d* mutant (Figs 1, 2). Studies using provascular markers lines, *ProAtHB8::GUS* and *ProAtHB8::YFP*, confirmed that the activity of vascular formation was enhanced in *hva-d* mutant. It remains to be determined whether HVA interacts genetically with the other three mutants in cambium development.

The activation of *HVA* (*AT5G27880*) is responsible for *hva-d* mutant phenotypes (Fig. 4). *HVA* gene encodes a putative transcription factor that belongs to the C2H2 zinc fingers superfamily comprising 176 members in *Arabidopsis*. Multiple sequence alignment of the most related proteins revealed high similarity in the conserved C2H2 domains and C-terminal conserved EAR motif. It has been shown that C2H2-type transcription factors play important roles in the regulation of plant growth, development, hormone responses, and tolerance to biotic and abiotic stresses (Ciftci-Yilmaz *et al.*, 2007; Kiełbowicz-Matuk, 2011). The EAR motif is crucial for transcriptional activity and mediates interaction with corepressors. HVA functions as a repressor, as shown in the transient expression assay (Fig. 5). Yeast two-hybrid assay and BiFC results confirmed that HVA protein interacts with TPL (Fig. 6a,b). Repression of the function of TPL restored bundle number of the *hva-d* mutant to WT, demonstrating that TPL function is necessary for HVA in controlling vascular development (Fig. 6c,d). By contrast, either mutation of the *HVA* gene with a CRISPR-cas approach or replacing EAR with an activation domain VP16 reduced the number of vascular bundles (Figs 7, S8). The HVA-VP16 transgenic lines showed a stronger phenotype than the CRISPR-cas lines probably due to the strong CaMV 35S promoter used to drive the expression of *HVA-VP16* construct. In addition, the potent VP16 activation domain may have caused activation of many HVA-related pathways. These biochemical and transgenic studies indicate that HVA positively regulates vascular formation in the stem. TPL interacts with EAR bearing transcription factors in various regulatory pathways involving auxin, jasmonate, and BR signaling (Causier *et al.*, 2012). Further investigation of genes and pathways downstream of the HVA-TPL pair may help to understand the regulatory mechanism of plant vascular bundle formation.

Auxin maxima controlled by polar auxin transport determine vascular bundles formation and spacing (Ibañes *et al.*, 2009). In this report, we found that the expression of *PIN1* was repressed by HVA, as shown by expression analysis and reporter line assay (Fig. 8a–c). Further EMSA experiment confirmed direct HVA binding to PIN1 promoter (Fig. 8d). The most substantial evidence of PIN1 involvement in HVA function came from genetics analysis, in which PIN1 is epistatic to HVA (Fig. 8h–l). Further, the *HVA-VP16* transgenic lines showed opposite phenotypes compared with *hva-d* mutant plants in vascular bundle number and *PIN1* expression (Fig. 8). As expected, auxin distribution was enhanced in the protoxylem regions in *hva-d* mutant (Fig. 9). The increased levels of *ProDR5::YFP* reporter and expanded expression region in the stem indicate changing auxin-response level and distribution in the *hva-d* mutant stem, which could also potentially explain the enhanced cambium activity. We therefore propose a functional model for HVA in regulating vascular bundle development, in which HVA represses *PIN1* expression and polar auxin transport, affects auxin distribution and potentially the number of auxin maxima in stem, promotes *AtHB8* expression, and as a result, enhances bundle number and cambium activity (Fig. 9h). It has been reported that *PIN1* expression precedes *AtHB8* expression (Scarpella *et al.*, 2006), and in turn AtHB8 may activate *PIN1* expression in a positive feedback loop (Miyashima *et al.*, 2013). In this study, we report that HVA functions as a negative regulator of *PIN1* expression, indicating that PIN1 is tightly modulated to ensure the formation of a proper vascular system (Fig. 9h).

PIN1 function is known to be regulated by phosphorylation (Zhang *et al.*, 2010; Li *et al.*, 2011; Huang *et al.*, 2012). Although this is beyond the scope of the current research, it would be interesting to see whether the phosphorylation status of PIN1 affects vascular development. In addition, BR signaling has been reported to modulate vascular bundle numbers by promoting early procambial cell formation in the shoot. Furthermore, mutations in CALAVATA (CLV) pathway genes lead to increased vascular bundle number as a result of the enlarged shoot meristem (DeYoung & Clark, 2008). In the future, it would be interesting to investigate whether there is a correlation between HVA-involved auxin distribution pathway and the BR and/or CLV pathways, which may further enhance our understanding of the function of the *HVA* gene in vascular development.

## Acknowledgements

We thank the *Arabidopsis* Biological Resource Center, Drs Thomas Greb, Yrjo Helariutta, and Li-Jia Qu for plant materials as detailed in the Materials and Methods section. Undergraduate students Alexander Francoeur, Gagganpreet Singh, Liam Iorio, and Tianyi Zhang participated in this research. This work was

supported by National Science Foundation (IOS-2049926), and in part, by USDA NIFA Hatch project #CONS01077 to HW.

## Competing interests

None declared.

## Author contributions

QD and HW designed the experiments. QD, BY, GTC, TW, LQ and HW performed the experiments. QD, BY, GTC, TW and HW analyzed the data. QD and HW wrote the article. QD, BY and GTC contributed equally to this work.

## ORCID

Huanzhong Wang https://orcid.org/0000-0002-9004-3420

## Data availability

The data that support the findings of this study are openly available in Biostudies at https://nam10.safelinks.protection.outlook.com/?url=https%3A%2F%2Fwww.ebi.ac.uk%2Fbiostudies%2F&data=05%7C02%7Chuanzhong.wang%40uconn.edu%7Cc33aae08060349a0f3db08dc9b756fb5%7C17f1a87e2a254eaab9df9d439034b080%7C0%7C0%7C638556176833555103%7CUnknown%7CTWFpbGZsb3d8eyJWIjoiMC4wLjAwMDAiLCJQIjoiV2luMzIiLCJBTiI6Ik1haWwiLCJXVCI6Mn0%3D%7C0%7C%7C%7C&sdata=tueMcOsiyvVu4UO77GGkZdGVLjyasEgXRJGghPzOb68%3D&reserved=0, reference no. E-MTAB-12850.

## References

**Agusti J, Herold S, Schwarz M, Sanchez P, Ljung K, Dun EA, Brewer PB, Beveridge CA, Sieberer T, Sehr EM *et al.* 2011.** Strigolactone signaling is required for auxin-dependent stimulation of secondary growth in plants. *Proceedings of the National Academy of Sciences, USA* **108**: 20242–20247.

**Baima S, Nobili F, Sessa G, Lucchetti S, Ruberti I, Morelli G. 1995.** The expression of the Athb-8 homeobox gene is restricted to provascular cells in *Arabidopsis thaliana*. *Development* **121**: 4171–4182.

**Benková E, Michniewicz M, Sauer M, Teichmann T, Seifertová D, Jürgens G, Friml J. 2003.** Local, efflux-dependent auxin gradients as a common module for plant organ formation. *Cell* **115**: 591–602.

**Brackmann K, Qi J, Gebert M, Jouannet V, Schlamp T, Grünwald K, Wallner ES, Novikova DD, Levitsky VG, Agustí J *et al.* 2018.** Spatial specificity of auxin responses coordinates wood formation. *Nature Communications* **9**: 1–15.

**Cano-Delgado A, Lee JY, Demura T. 2010.** Regulatory mechanisms for specification and patterning of plant vascular tissues. *Annual Review of Cell and Developmental Biology* **26**: 605–637.

**Causier B, Ashworth M, Guo W, Davies B. 2012.** The TOPLESS interactome: a framework for gene repression in Arabidopsis. *Plant Physiology* **158**: 423–438.

**Cheng Y, Dai X, Zhao Y. 2006.** Auxin biosynthesis by the YUCCA flavin monooxygenases controls the formation of floral organs and vascular tissues in Arabidopsis. *Genes & Development* **20**: 1790–1799.

**Ciftci-Yilmaz S, Morsy MR, Song L, Coutu A, Krizek BA, Lewis MW, Warren D, Cushman J, Connolly EL, Mittler R. 2007.** The EAR-motif of the Cys2/His2-type zinc finger protein Zat7 plays a key role in the defense response of Arabidopsis to salinity stress. *The Journal of Biological Chemistry* **282**: 9260–9268.

**DeYoung BJ, Clark SE. 2008.** BAM receptors regulate stem cell specification and organ development through complex interactions with CLAVATA signaling. *Genetics* **180**: 895.

**Donner TJ, Sherr I, Scarpella E. 2009.** Regulation of preprocambial cell state acquisition by auxin signaling in Arabidopsis leaves. *Development* **136**: 3235–3246.

**Du Q, Avci U, Li S, Gallego-Giraldo L, Pattathil S, Qi L, Hahn MG, Wang H. 2015.** Activation of miR165b represses AtHB15 expression and induces pith secondary wall development in Arabidopsis. *The Plant Journal* **83**: 388–400.

**Englbrecht CC, Schoof H, Bohm S. 2004.** Conservation, diversification and expansion of $C_2H_2$ zinc finger proteins in the *Arabidopsis thaliana* genome. *BMC Genomics* **5**: 39.

**Fàbregas N, Formosa-Jordan P, Confraria A, Siligato R, Alonso JM, Swarup R, Bennett MJ, Mähönen AP, Caño-Delgado AI, Ibañes M. 2015.** Auxin influx carriers control vascular patterning and xylem differentiation in *Arabidopsis thaliana*. *PLoS Genetics* **11**: e1005183.

**Fàbregas N, Ibañes M, Caño-Delgado AI. 2010.** A systems biology approach to dissect the contribution of brassinosteroid and auxin hormones to vascular patterning in the shoot of *Arabidopsis thaliana*. *Plant Signaling & Behavior* **5**: 903–906.

**Fujita D, Trijatmiko KR, Tagle AG, Sapasap MV, Koide Y, Sasaki K, Tsakirpaloglou N, Gannaban RB, Nishimura T, Yanagihara S *et al.* 2013.** NAL1 allele from a rice landrace greatly increases yield in modern indica cultivars. *Proceedings of the National Academy of Sciences, USA* **110**: 20431–20436.

**Gälweiler L, Guan C, Müller A, Wisman E, Mendgen K, Yephremov A, Palme K. 1998.** Regulation of polar auxin transport by AtPIN1 in Arabidopsis vascular tissue. *Science* **282**: 2226–2230.

**Guo Y, Qin G, Gu H, Qu LJ. 2009.** Dof5.6/HCA2, a Dof transcription factor gene, regulates interfascicular cambium formation and vascular tissue development in Arabidopsis. *Plant Cell* **21**: 3518–3534.

**He JX, Gendron JM, Sun Y, Gampala SS, Gendron N, Sun CQ, Wang ZY. 2005.** BZR1 is a transcriptional repressor with dual roles in brassinosteroid homeostasis and growth responses. *Science* **307**: 1634–1638.

**Hiratsu K, Ohta M, Matsui K, Ohme-Takagi M. 2002.** The SUPERMAN protein is an active repressor whose carboxy-terminal repression domain is required for the development of normal flowers. *FEBS Letters* **514**: 351–354.

**Huang F, Zago MK, Abas L, van Marion A, Galván-Ampudia CS, Offringa R. 2012.** Phosphorylation of conserved PIN motifs directs Arabidopsis PIN1 polarity and auxin transport. *Plant Cell* **22**: 1129–1142.

**Hunziker P, Greb T. 2024.** Stem cells and differentiation in vascular tissues. *Annual Review of Plant Biology* **75**: 11.1–11.27.

**Ibañes M, Fàbregas N, Chory J, Caño-Delgadob AI. 2009.** Brassinosteroid signaling and auxin transport are required to establish the periodic pattern of Arabidopsis shoot vascular bundles. *Proceedings of the National Academy of Sciences, USA* **106**: 13630–13635.

**Ilegems M, Douet V, Meylan-Bettex M, Uyttewaal M, Brand L, Bowman JL, Stieger PA. 2010.** Interplay of auxin, KANADI and Class III HD-ZIP transcription factors in vascular tissue formation. *Development* **137**: 975–984.

**Kagale S, Rozwadowski K. 2011.** EAR motif-mediated transcriptional repression in plants: an underlying mechanism for epigenetic regulation of gene expression. *Epigenetics* **6**: 141.

**Ke J, Ma H, Gu X, Thelen A, Brunzelle JS, Li J, Xu HE, Melcher K. 2015.** Structural basis for recognition of diverse transcriptional repressors by the TOPLESS family of corepressors. *Science Advances* **1**: e1500107.

**Kiełbowicz-Matuk A. 2011.** Involvement of plant C(2)H(2)-type zinc finger transcription factors in stress responses. *Plant Science* **185–186**: 78–85.

**Li H, Lin D, Dhonukshe P, Nagawa S, Chen D, Friml J, Scheres B, Guo H, Yang Z. 2011.** Phosphorylation switch modulates PIN1 localization in PCs 970 Phosphorylation switch modulates the interdigitated pattern of PIN1 localization and cell expansion in Arabidopsis leaf epidermis. *Cell Research* **21**: 970–978.

**Long JA, Ohno C, Smith ZR, Meyerowitz EM. 2006.** TOPLESS regulates apical embryonic fate in Arabidopsis. *Science* **312**: 1520–1523.

**Mahonen AP, Bonke M, Kauppinen L, Riikonen M, Benfey PN, Helariutta Y. 2000.** A novel two-component hybrid molecule regulates vascular morphogenesis of the Arabidopsis root. *Genes & Development* **14**: 2938–2943.

**Marquès-Bueno MM, Morao AK, Cayrel A, Platre MP, Barberon M, Caillieux E, Colot V, Jaillais Y, Roudier F, Vert G. 2016.** A versatile multisite gateway-compatible promoter and transgenic line collection for cell type-specific functional genomics in Arabidopsis. *The Plant Journal* **85**: 320–333.

**Miyashima S, Sebastian J, Lee JY, Helariutta Y. 2013.** Stem cell function during plant vascular development. *EMBO Journal* **32**: 178–193.

**Ohashi-Ito K, Saegusa M, Iwamoto K, Oda Y, Katayama H, Kojima M, Sakakibara H, Fukuda H. 2014.** A bHLH complex activates vascular cell division via cytokinin action in root apical meristem. *Current Biology* **24**: 2053–2058.

**Ohta M, Matsui K, Hiratsu K, Shinshi H, Ohme-Takagi M. 2001.** Repression domains of class II ERF transcriptional repressors share an essential motif for active repression. *Plant Cell* **13**: 1959–1968.

**Osmont KS, Hardtke CS. 2008.** The topless plant developmental phenotype explained! *Genome Biology* **9**: 1–4.

**Parker G, Schofield R, Sundberg B, Turner S. 2003.** Isolation of COV1, a gene involved in the regulation of vascular patterning in the stem of Arabidopsis. *Development* **130**: 2139–2148.

**Pineau C, Freydier A, Ranocha P, Jauneau A, Turner S, Lemonnier G, Renou JP, Tarkowski P, Sandberg G, Jouanin L *et al.* 2005.** HCA: an Arabidopsis mutant exhibiting unusual cambial activity and altered vascular patterning. *The Plant Journal* **44**: 271–289.

**Rolland-Lagan AG, Prusinkiewicz P. 2005.** Reviewing models of auxin canalization in the context of leaf vein pattern formation in Arabidopsis. *The Plant Journal* **44**: 854–865.

**Sachs T. 1981.** The control of the patterned differentiation of vascular tissues. *Advances in Botanical Research* **9**: 151–262.

**Sachs T. 2000.** Integrating cellular and organismic aspects of vascular differentiation. *Plant and Cell Physiology* **41**: 649–656.

**Scarpella E, Marcos D, Friml J, Berleth T. 2006.** Control of leaf vascular patterning by polar auxin transport. *Genes and Development* **20**: 1015–1027.

**Schwab R, Ossowski S, Riester M, Warthmann N, Weigel D. 2006.** Highly specific gene silencing by artificial microRNAs in Arabidopsis. *Plant Cell* **18**: 1121–1133.

**Seipel K, Georgiev O, Schaffner W. 1994.** A minimal transcription activation domain consisting of a specific array of aspartic acid and leucine residues. *Biological Chemistry Hoppe-Seyler* **375**: 463–470.

**Shih CF, Hsu WH, Peng YJ, Yang CH. 2014.** The NAC-like gene ANTHER INDEHISCENCE FACTOR acts as a repressor that controls anther dehiscence by regulating genes in the jasmonate biosynthesis pathway in Arabidopsis. *Journal of Experimental Botany* **65**: 621–639.

**Smetana O, Mäkilä R, Lyu M, Amiryousefi A, Sánchez Rodríguez F, Wu MF, Solé-Gil A, Leal Gavarrón M, Siligato R, Miyashima S *et al.* 2019.** High levels of auxin signalling define the stem-cell organizer of the vascular cambium. *Nature* **565**: 485–489.

**Song CP, Galbraith DW. 2006.** AtSAP18, an orthologue of human SAP18, is involved in the regulation of salt stress and mediates transcriptional repression in Arabidopsis. *Plant Molecular Biology* **60**: 241–257.

**Stuttmann J, Barthel K, Martin P, Ordon J, Erickson JL, Herr R, Ferik F, Kretschmer C, Berner T, Keilwagen J *et al.* 2021.** Highly efficient multiplex editing: one-shot generation of 8x *Nicotiana benthamiana* and 12x Arabidopsis mutants. *The Plant Journal* **106**: 8–22.

**Suer S, Agusti J, Sanchez P, Schwarz M, Greb T. 2011.** WOX4 imparts auxin responsiveness to cambium cells in Arabidopsis. *Plant Cell* **23**: 3247.

**Sun S, Liu Z, Wang X, Song J, Fang S, Kong J, Li R, Wang H, Cui X. 2024.** Genetic control of thermomorphogenesis in tomato inflorescences. *Nature Communications* **15**: 1–10.

**Szemenyei H, Hannon M, Long JA. 2008.** TOPLESS mediates auxin-dependent transcriptional repression during Arabidopsis embryogenesis. *Science* **319**: 1384–1386.

**Tiwari SB, Hagen G, Guilfoyle TJ. 2004.** Aux/IAA proteins contain a potent transcriptional repression domain. *Plant Cell* **16**: 533–543.

**Tonn N, Greb T. 2017.** Radial plant growth. *Current Biology* **27**: R878–R882.

**Tuominen H, Puech L, Fink S, Sundberg B. 1997.** A radial concentration gradient of indole-3-acetic acid is related to secondary xylem development in hybrid aspen. *Plant Physiology* **115**: 577–585.

**Turner S, Sieburth LE. 2003.** Vascular patterning. *The Arabidopsis Book* **2**: e0073.

**Wang H. 2024.** Endogenous and environmental signals in regulating vascular development and secondary growth. *Frontiers in Plant Science* **15**: 1369241.

**Wang L, Kim J, Somers DE. 2013.** Transcriptional corepressor TOPLESS complexes with pseudoresponse regulator proteins and histone deacetylases to regulate circadian transcription. *Proceedings of the National Academy of Sciences, USA* **110**: 761–766.

**Wang S, Wang H. 2020.** Coordination of multilayered signalling pathways on vascular cambium activity. *Annual Plant Reviews Online* **3**: 457–472.

**Weigel D, Ahn JH, Blázquez MA, Borevitz JO, Christensen SK, Fankhauser C, Ferrándiz C, Kardailsky I, Malancharuvil EJ, Neff MM *et al.* 2000.** Activation tagging in Arabidopsis. *Plant Physiology* **122**: 1003–1013.

**Wenzel CL, Schuetz M, Yu Q, Mattsson J. 2007.** Dynamics of MONOPTEROS and PIN-FORMED1 expression during leaf vein pattern formation in *Arabidopsis thaliana*. *The Plant Journal* **49**: 387–398.

**Ye L, Wang X, Lyu M, Siligato R, Eswaran G, Vainio L, Blomster T, Zhang J, Mähönen AP. 2021.** Cytokinins initiate secondary growth in the Arabidopsis root through a set of LBD genes. *Current Biology* **31**: 3365–3373.

**Yin Y, Wang ZY, Mora-Garcia S, Li J, Yoshida S, Asami T, Chory J. 2002.** BES1 accumulates in the nucleus in response to brassinosteroids to regulate gene expression and promote stem elongation. *Cell* **109**: 181–191.

**Zhang J, Nodzyński T, Pěnčík A, Rolčík J, Friml J. 2010.** PIN phosphorylation is sufficient to mediate PIN polarity and direct auxin transport. *Proceedings of the National Academy of Sciences, USA* **107**: 918–922.

## Supporting Information

Additional Supporting Information may be found online in the Supporting Information section at the end of the article.

**Fig. S1** Plant growth phenotypes of *hva-d* mutant plants.

**Fig. S2** Characterization of a phloem marker *ProAPL:GUS* in *hva-d* mutant plants.

**Fig. S3** Characterization of plants overexpressing *At5g27889* and *At5g27890*.

**Fig. S4** Sequence analysis of HVA/At5g27880 and its orthologs.

**Fig. S5** Subcellular localization of eGFP-HVA and expression of *ProHVA:GUS* in transgenic Arabidopsis plants.

**Fig. S6** Characterization of plants overexpressing *HVA* without Ethylene-responsive element binding factor-associated Amphiphilic Repression domain.

**Fig. S7** Yeast two-hybrid analysis of interaction between HVA and SAP18.

**Fig. S8** Generating mutations in HVA gene using a CRISPR-Cas9 gene editing approach.

**Fig. S9** Overexpression of an *HVA-VP16* construct in wild-type plants.

**Fig. S10** Plant growth phenotypes of the double mutant *pin1 HVA-VP16*.

**Fig. S11** Characterization of the *PIN1:PIN1-GFP* reporter in different backgrounds.

**Fig. S12** NPA treatment increases *ProDR5:YFP* signal and cambial cell activity.

**Table S1** Primers used in this research.

**Table S2** Result of the microarray analysis of *hva-d* mutant.

Please note: Wiley is not responsible for the content or functionality of any Supporting Information supplied by the authors. Any queries (other than missing material) should be directed to the *New Phytologist* Central Office.